J|A|C|S

A R T I C L E S

Proton Transfer and a Dielectric Phase Transition in the Molecular Conductor (HDABCO$^+$)$_2$(TCNQ)$_3$

Tomoyuki Akutagawa,*,†,§ Sadamu Takeda,‡ Tatsuo Hasegawa,† and Takayoshi Nakamura*,†,§

Contribution from the Research Institute for Electronic Science, Hokkaido University, Sapporo 060-0812, Japan, Graduate School of Science, Hokkaido University, Sapporo 060-0810, Japan, and CREST, Japan Science and Technology Corporation (JST), Kawaguchi 332-0012, Japan

Received August 5, 2003; E-mail: takuta@imd.es.hokudai.ac.jp

Abstract: One-dimensional dielectric (N···H···N)$_\infty$ hydrogen-bonding chains of monoprotonated 1,4-diazabicyclo[2.2.2]octane (HDABCO$^+$) were introduced into an electrically conducting 7,7,8,8-tetracyano-*p*-quinodimethane (TCNQ) salt as the countercation structure. Room-temperature electrical conductivity was ~10^{-3} S cm^{-1}, with a semiconductive behavior. The temperature-dependent dielectric constants of (HDABCO$^+$)$_2$(TCNQ)$_3$ indicated a dielectric transition at 306 K. A large deuterium isotope effect for the dielectric transition ($\Delta T = 70$ K) was observed for the deuterated salt, (DDABCO$^+$)$_2$(TCNQ)$_3$. Thermally activated order/disorder of the protons or deuteriums within the one-dimensional hydrogen-bonding chains of (HDABCO$^+$)$_\infty$ and (DDABCO$^+$)$_\infty$ affected the dielectric responses in the TCNQ-based semiconductors.

Introduction

Hydrogen bonds within molecular complexes can be appropriately designed to realize dynamic protonic motion,[1,2] which plays an important role in causing the phase transition of hydrogen-bonding dielectrics.[3,4] For example, several photo- and thermally induced intramolecular proton-transfer (PT) processes within the single crystals of 6-(2,4-dinitrobenzyl)-2,2′-bipyridine have resulted in a multiconvertible optical material.[1a] Upon irradiation using visible light, the intramolecular PT process of 6-(2,4-dinitrobenzyl)-2,2′-bipyridine caused the appearance of the crystals to shift from colorless to blue, which can then be restored to the colorless form by thermal treatment. Similarly, reversible photo- and thermally induced PT processes were observed for the intermolecular PT processes of [*meso*-1,2-bis-(4-dimethylaminophenyl)-1,2-ethanediol][bis-(4-cyanobenzylidene)ethylenediamine], in which photoexcitation of the intermolecular CT absorption of the charge-transfer (CT) complex caused a shift of its appearance from pale yellow to black (ionic form) and was reversed by thermal treatment.[1b] The

optical properties of these crystals can be independently controlled by photoirradiation and thermal treatment.

The crystals possess other interesting PT processes such as proton relay through hydrogen-bonding networks and proton–electron hybrid conductive behavior in hydrogen-bonding molecular conductors.[2c] External stimuli, such as photoirradiation, heat, and electrical field, have been shown to cause changes in the intra- and intermolecular hydrogen-bonding environments. In the cases where the hydrogen-bonding interactions are associated with π-conjugated molecular systems, the PT processes modulated the electronic structures of the π-electron system as outputs of thermochromism, photochromism, and long-range protonic motion. Although a large number of ferro- and antiferroelectric materials with low molecular weights in liquid crystalline compounds have been developed,[5] reports on the hydrogen-bonding dielectrics in the form of single crystals have only recently become available. Examples of hydrogen-bonding dielectrics with long-range ordering of the dipole arrangement include the antiferroelectric phase transition exhibited by squaric acid and the ferroelectric phase transition of monoprotonated 1,4-diazabicyclo[2.2.2]octane (HDABCO$^+$) salts.[4,6a−c] Electrically active molecular systems can be realized by the introduction of these novel hydrogen-bonding dielectrics into open-shell π-electron systems, which can generate conduction carriers or magnetic spins such as those observed in molecular conductors and magnets. Consequently, HDABCO$^+$

† Research Institute for Electronic Science, Hokkaido University.
‡ Graduate School of Science, Hokkaido University.
§ CREST, Japan Science and Technology Corporation.
(1) (a) Eichen, Y.; Lehn, J.-M.; Scherl, M.; Haarer, D.; Fischer, J.; DeCian, A.; Corval, A.; Trommsdorff, H. P. *Angew. Chem., Int. Ed. Engl.* **1995**, *34*, 2530. (b) Felderhoff, M.; Steller, I.; Reyes-Arellano, A.; Boese, R.; Sustmann, R. *Adv. Mater.* **1996**, *8*, 402.
(2) (a) Akutagawa, T.; Saito, G. *Bull. Chem. Soc. Jpn.* **1995**, *68*, 1753. (b) Akutagawa, T.; Saito, G.; Kusunoki, M.; Sakaguchi, K. *Bull. Chem. Soc. Jpn.* **1996**, *69*, 2487. (c) Akutagawa, T.; Hasegawa, T.; Nakamura, T.; Inabe, T.; Saito, G. *Chem.—Eur. J.* **2002**, *8*, 4402.
(3) (a) Lines, M. E.; Glass, A. M. *Principles and Applications of Ferroelectric and Related Materials*; Clarendon Press: Oxford, 1977. (b) Jona, F.; Shirane, G. *Ferroelectric Crystals*; Dover Publications Inc.: New York, 1993.
(4) Katrusiak, A.; Szafranski, M. *Phys. Rev. Lett.* **1999**, *82*, 576.

(5) Collings, P. J.; Hird, M. *Introduction to Liquid Crystals: Chemistry and Physics*; Taylor & Francis: Philadelphia, 1997.
(6) (a) Semmingsen, D.; Feder, J. *Solid State Commun.* **1974**, *15*, 1369. (b) Semmingsen, D.; Hollander, F. J.; Ketzle, T. F. *J. Phys. Chem.* **1979**, *66*, 4405. (c) Samara, G. A.; Semmingsen, D. *J. Chem. Phys.* **1979**, *71*, 1401. (d) Terao, H.; Sugawara, T.; Kita, Y.; Sato, N.; Kaho, E.; Takeda, S. *J. Am. Chem. Soc.* **2001**, *123*, 10468.

Scheme 1. Equilibrium among the Three Ionization States of 1,4-Diazabicyclo[2.2.2]octane (DABCO)
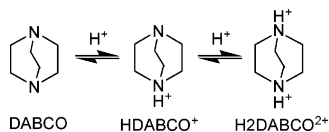
molecules were introduced as the dielectric units into the open-shell π-electron systems.

A DABCO molecule possesses two proton-accepting nitrogen sites with $pK_{a1} = 8.82$ and $pK_{a2} = 2.97$ (Scheme 1).[7] Among the three ionization states, the salts of the monoprotonated HDABCO$^+$ cation, such as (HDABCO$^+$)(BF$_4^-$) and (HDABCO$^+$)(ClO$_4^-$), formed one-dimensional (1D) (N−H$^+$···N)$_\infty$ hydrogen-bonding chains, accompanied by a ferroelectric phase transition that is associated with the PT process.[4] In the ferroelectric phase, the thermally fluctuating protons between the two nitrogen sites of DABCO were ordered in the 1D (HDABCO)$_\infty$ chain, which generated the long-range dipole arrangements of the HDABCO$^+$ molecules along the hydrogen-bonding chain. The resulting dynamic motion of the protons in the 1D hydrogen-bonding dielectric units of the (HDABCO$^+$)$_\infty$ chain is a notable countercation structure,[8] which can be introduced into the open-shell π-electron structures of the molecular conductors. Herein, we report a first example of a molecular semiconductor featuring the incorporation of 1D hydrogen-bonding dielectric chains into the electrically conducting 7,7,8,8-tetracyano-p-quinodimethane (TCNQ) salt as the CT complexes (HDABCO$^+$)$_2$(TCNQ)$_3$ and deuterated (DDABCO$^+$)$_2$-(TCNQ)$_3$ (salts **1** and **2**, respectively).

Experimental Section

Preparation of Salts 1 and 2. The metathesis reaction between Li(TCNQ) and (HDABCO)(BF$_4^-$) in CH$_3$CN−H$_2$O (8:2) afforded the single crystals of salt **1** as black plates. Anal. calcd for C$_{24}$H$_{19}$N$_8$ (419.47): C, 68.72; H, 4.57; N, 26.71. Found: C, 69.02; H, 4.73; N, 26.65. Similarly, single crystals of salt **2** were obtained as black plates using Li(TCNQ) and (DDABCO$^+$)(Cl$^-$) in C$_2$D$_5$OD−D$_2$O (8:2). Anal. calcd for C$_{24}$H$_{19}$N$_8$ (419.47): C, 68.72; H, 4.57; N, 26.71. Found: C, 68.85; H, 4.64; N, 26.51.

Electrical Measurements. Temperature-dependent dielectric constants were measured by the two-probe AC impedance method over the frequency range from 100 to 10 × 10^6 Hz (HP4194A). The single crystals were placed into a cryogenic refrigerating system (Daikin PS24SS). Temperature-dependent electrical conductivities were measured along the long axis of the crystal by the DC four-probe method. The stacking direction of the TCNQ molecules was aligned along the long axis of the crystal. Electrical contacts were prepared using gold paste to attach the 10-μm ϕ gold wires to the crystals (Tokuriki 8560).

Optical Spectra. Infrared (IR, 400−7600 cm^{-1}) spectra measurements were carried out on KBr pellets using a Perkin-Elmer Spectrum 2000 spectrophotometer with a resolution of 1 cm^{-1}. UV−vis−NIR spectra (350−3200 nm) were measured as KBr pellets using a Perkin-Elmer λ-19 spectrophotometer with a resolution of 8 nm.

Calculation of Transfer Integrals. The transfer integrals (t) and band structures were calculated within the tight-binding approximation using the extended Hückel molecular orbital method.[9] The LUMO of the TCNQ molecule was used as the basis function. Semiempirical parameters for Slater-type atomic orbitals were used. The t values

(7) Gunzonas, D. A.; Irish, D. E. *Can. J. Chem.* **1988**, *66*, 1249.
(8) Bandrauk, A. D.; Ishii, K.; Aubin, T. M.; Hanson, A. W. *J. Phys. Chem.* **1985**, *89*, 1478.
(9) Mori, T.; Kobayashi, A.; Sasaki, Y.; Kobayashi, H.; Saito, G.; Inokuchi, H. *Bull. Chem. Soc. Jpn.* **1984**, *57*, 627.

between each pair of molecules were assumed to be proportional to the overlap integral (S) as defined by the equation, $t = -10S$ eV.

Solid-State ^{13}C NMR. ^{13}C-MAS NMR spectra of salt **1** were measured using a single-pulse method with a Bruker DSX300 spectrometer and a 4-mm CP/MAS probe between 296 and 320 K. A conventional zirconia rotor (4 mm) with a boron nitride cap was used. To achieve a homogeneous temperature at the sample position, the specimen (ca. 10−20 mg) was carefully packed at the center of the rotor (2−3 mm long). Teflon powder was used as the spacer.

X-ray Structural Analysis. Crystallographic data were collected using a Rigaku Raxis-Rapid diffractometer with Mo Kα ($\lambda = 0.71073$ Å) radiation from a graphite monochromator. Structure refinements were performed using the full-matrix least-squares method on F^2. Calculations were performed using Crystal Structure software packages.[10] Parameters were refined using anisotropic temperature factors, with the exception of those for the hydrogen atom. The positions of the hydrogens were determined by differential Fourier analysis. Crystal data of salt **1**: C$_{24}$H$_{19}$N$_8$, FW 419.47, black plate, $T = 100$ K, space group $P\bar{1}$ (#2), $a = 7.607(4)$, $b = 10.097(1)$, $c = 13.895(1)$ Å, $\alpha = 89.4(2)$, $\beta = 84.063(3)$, $\gamma = 70.988(3)°$, $V = 1023.6(1)$ Å^3, $Z = 2$, $\rho_{calcd} = 1.361$ g cm^{-3}, 7476 measured, 4273 unique, 3050 observed ($I > 2.0\sigma(I)$), $R = 0.056$, $R_w = 0.097$, GOF = 0.440. $T = 373$ K, $a = 7.8164(7)$, $b = 10.3585(3)$, $c = 14.020(1)$ Å, $\alpha = 88.8(2)$, $\beta = 83.944(3)$, $\gamma = 69.911(3)°$, $V = 1060.0(1)$ Å^3, $Z = 2$, $\rho_{calcd} = 1.314$ g cm^{-3}, 8124 measured, 4415 unique, 2309 observed ($I > 2.0\sigma(I)$), $R = 0.073$, $R_w = 0.072$, GOF = 0.674. Crystal data of salt **2**: C$_{24}$H$_{18}$DN$_8$, FW 420.47, black plate, $T = 100$ K, space group $P\bar{1}$ (#2), $a = 7.8153(5)$, $b = 10.1860(3)$, $c = 14.0200(7)$ Å, $\alpha = 89.5(2)$, $\beta = 84.021(3)$, $\gamma = 70.743(3)°$, $V = 1047.5(1)$ Å^3, $Z = 2$, $\rho_{calcd} = 1.330$ g cm^{-3}, 8347 measured, 4475 unique, 2984 observed ($I > 2.0\sigma(I)$), $R = 0.052$, $R_w = 0.042$, GOF = 0.429. $T = 373$ K, space group $P\bar{1}$ (#2), $a = 7.851(1)$, $b = 10.454(2)$, $c = 14.074(3)$ Å, $\alpha = 88.8(2)$, $\beta = 83.455(8)$, $\gamma = 69.668(7)°$, $V = 1075.8(3)$ Å^3, $Z = 2$, $\rho_{calcd} = 1.295$ g cm^{-3}, 7343 measured, 4266 unique, 2006 observed ($I > 2.0\sigma(I)$), $R = 0.069$, $R_w = 0.088$, GOF = 0.90.

Results and Discussion

Formation of the CT complexes of (HDABCO$^+$)$_2$(TCNQ)$_3$ and deuterated (DDABCO$^+$)$_2$(TCNQ)$_3$ (salts **1** and **2**, respectively) were carried out using the metathesis reaction. Except for the position of the heavy hydrogen atoms, the structure of deuterated salt **2** was identical to that of salt **1**. X-ray crystal structural analysis allowed the determination of the temperature-dependent changes in the position of the proton within the hydrogen-bonding chain. The dielectric and hydrogen-bonding properties of salt **1** were evaluated using temperature-dependent dielectric constants, isotope effects, and solid-state ^{13}C NMR spectra.

Crystal Structures. The unit cell of salt **1** ($T = 100$ K) viewed along the $-a + b$ axis is shown in Figure 1a. Segregated nonuniform TCNQ stacks were observed along the $-a + b$ axis. Two types of TCNQ molecules (**A** and **B**) were stacked in the π-stacking sequence of (**A**−**B**−**A**)$_\infty$. The magnitude of the intermolecular interactions within the TCNQ stack was evaluated using the intermolecular transfer integral (t, eV). Since the intermolecular **A**−**A** interaction ($t_1 = 21.7 \times 10^{-2}$ eV) was roughly 1 order of magnitude greater than the **A**−**B** interaction ($t_2 = -3.4 \times 10^{-2}$ eV), the intermolecular interactions were dominated by the **A**−**A** dimers.

HDABCO$^+$ cations formed 1D (N···H···N)$_\infty$ hydrogen-bonding chains that were parallel to the TCNQ stacks (Figure

(10) *Crystal Structure*, version 3.1; single-crystal structure analysis software; Rigaku Corporation and Molecular Structure Corporation: Tokyo, Japan, 2003.
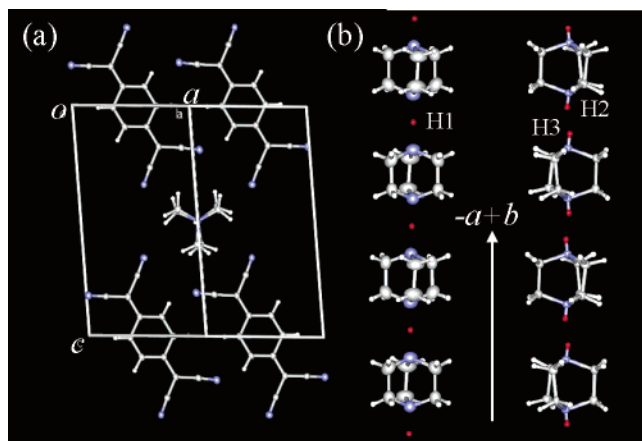
Figure 1. Crystal structure of $(HDABCO^+)_2(TCNQ)_3$ (**1**). (a) Unit cell viewed along the $-a + b$ axis ($T = 100$ K). (b) One-dimensional $(N \cdots H \cdots N)_\infty$ hydrogen-bonded structures at 373 K (left) and at 100 K (right). The hydrogen-bonding protons are shown in red. At 373 K, the proton H1 was observed near the midpoint between the two nitrogen atoms (left), whereas at 100 K, the proton was observed at the localized sites H2 and H3 (right).

1). The crystal structural analyses of salt **1** revealed two hydrogen-bonding protonic sites (H2 and H3) at 100 K, which were observed to merge at 373 K into one site (H1) at the midpoint between the two nitrogen atoms. If the time scale of the measurements is shorter than the correlation time of the thermal fluctuation for hydrogen-bonding protons, it is possible that the $H2DABCO^{2+}$ or DABCO states are formed in the 1D $HDABCO^+$ hydrogen-bonding chain at 373 K. Since the disproportional $[(H2DABCO^{2+}) - (DABCO)]_\infty$ hydrogen-bonding structure should be unstable,[11] the protons at 100 K should localize at either the H2 or H3 protonic sites. Accordingly, $HDABCO^+$ should be the dominant chemical species at 100 K. The localization of the protonic lattice of $(HDABCO^+)_\infty$ at 100 K gave rise to a dipole structure within the 1D hydrogen-bonding chain, which was reflected in the dielectric properties. In contrast, the thermally fluctuating proton between the two nitrogen sites should eliminate the dipole structure within the chain.

Dielectric Properties. The temperature-dependent dielectric constants (ϵ_1) of salts **1** and **2** at a fixed frequency of 100 kHz are shown in Figure 2. At roughly 306 K, a sharp dielectric peak of salt **1** was observed along the $-a + b$ axis, but not along the *c*-axis. The dielectric response at 306 K should, therefore, be associated with the hydrogen bonds along the $-a + b$ axis. On the other hand, the dielectric peak of deuterated salt **2** was observed at 376 K with a large deuterium isotope effect ($\Delta T = 70$ K). The results indicated a correlation between the hydrogen-bonding structure and the dielectric properties. The average N–N distance in the $N-D^+ \cdots N$ hydrogen bond of salt **2** (2.801 Å) was slightly longer than that of salt **1** (2.789 Å).

From the stoichiometry of salts **1** and **2**, the formal charge on each TCNQ molecule was calculated as 0.67 electron. The partial charge-transfer of the electronic structure of the TCNQ molecule was confirmed by the appearance of an intermolecular CT transition at approximately 3.5×10^3 cm^{-1}.[12] Room-temperature electrical conductivities of salts **1** and **2** were 5 ×
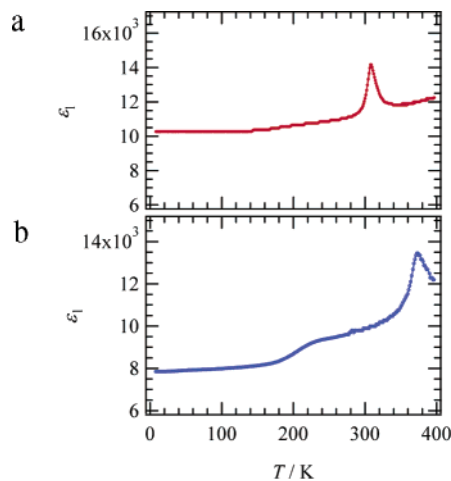

Figure 2. Temperature-dependent dielectric constants ($T-\epsilon_1$ plots) of salts **1** (a) and **2** (b), measured at a fixed frequency 100 kHz. The values for ϵ_1 were measured along the $-a + b$ axis.

10^{-3} ($E_a = 0.28$ eV) and 1×10^{-2} S cm^{-1} ($E_a = 0.25$ eV), respectively. Our results show a correlation between the semiconducting temperature dependences and the nonuniform stacking structure of the TCNQ stack.

Dielectric Properties and Hydrogen Bonds. Our results have demonstrated a correlation between the dielectric properties of salts **1** and **2** and the 1D $HDABCO^+$ hydrogen-bonding behaviors. Since the dielectric transitions occurred at relatively high temperatures, it is reasonable to describe the mechanism as the thermally induced order/disorder transition of the hydrogen-bonding protons rather than by quantum tunneling.[3,11,13] The dielectric responses can be affected by the thermally activated localization/delocalization (order/disorder) of the protons or deuteriums within the hydrogen-bonding chains. To clarify the local electronic structure of the TCNQ molecules in the vicinity of the temperature of dielectric transition (T_c), high-resolution solid-state ^{13}C NMR spectra of salt **1** were measured at 296 and 320 K. Both ^{13}C NMR spectra indicated changes in the CT state of TCNQ around the dielectric transition. The absence of several peaks in the disordered phase ($T > 306$ K),[14] which were assigned to the TCNQ molecules in the ordered phase ($T < 306$ K), suggested changes in the local magnetic field around the TCNQ molecules as the result of increasing the temperature above the dielectric transition. The negative charges on the TCNQ molecules should be affected by the 1D hydrogen-bonding cation structures through the electrostatic interactions between the $HDABCO^+$ cations and the TCNQ anions. It is, therefore, reasonable to expect that the dielectric phase transitions of 1D $HDABCO^+$ hydrogen-bonding chains would modulate the electronic structures of TCNQ.

Schematic illustrations of possible double-well potential curves of the protons in the infinite 1D hydrogen-bonding chains are shown in Figure 3. Strong hydrogen bonds ($N-H^+ \cdots N$), with N–N distances less than 2.5 Å, typically exhibit a single-

(11) (a) Jeffrey, G. A. *An Introduction to Hydrogen Bonding*; Truhlar, D. G., Ed.; Oxford University Press: New York, 1997. (b) Katrusiak, A.; Ratajczak-Sitarz, M.; Crech, E. *J. Mol. Struct.* **1999**, *474*, 135.

(12) (a) Torrance, J. B.; Scott, B. A.; Kaufman, F. B. *Solid State Commun.* **1975**, *17*, 1369. (b) Torrance, J. B.; Scot, B. A.; Welber, B.; Kaufman, F. B.; Seiden, P. E. *Phys. Rev. B* **1979**, *19*, 730. (c) Jacobsen, C. S. *Optical Properties in Semiconductor and Semimetals. High Conducting Quasi-One-Dimensional Organic Crystals*; Conwell, E., Ed.; Academic Press: New York, 1988; p 293.

(13) Steiner, T. *Angew. Chem., Int. Ed.* **2002**, *41*, 48.

(14) Nune, T.; Vainrub, A.; Ribet, M.; Rachdi, F.; Bernier, P.; Almeida, M. *J. Chem. Phys.* **1992**, *98*, 8021.
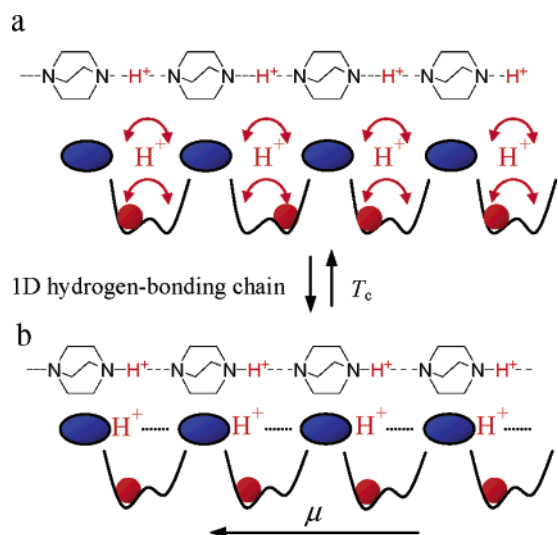
Figure 3. Schematic illustration of double-well proton coordinates along the 1D hydrogen-bonding chain: (a) high-temperature ($T > 306$ K) and (b) low-temperature ($T < 306$ K) phases.

well potential curve of proton coordinate.[13] However, the observed N−N distances for salts **1** and **2** (∼2.8 Å) lie within the range of double-well potential curves of the proton coordinate, and therefore, the protons at the higher temperature regions ($T > 306$ K) should thermally fluctuate between two double-well potentials of proton coordinates (Figure 3a). Accordingly, X-ray structural analysis indicated that the time-resolved average proton coordinate was located at approximately the midpoint between the two nitrogen sites. At temperatures below 306 K, the thermally fluctuating protons were fixed at one of the minimum positions within the hydrogen bond, which resulted in the ordered $[\text{N−H}^+\cdots\text{N}]_\infty$ dipole arrangement of 1D infinite (HDABCO$^+$)$_\infty$ chain (Figure 3b). In the cases of the thermally activated PT processes, a correlation was observed between the T_c values and the barrier height of double-well potential curves of the proton coordinate. Subsequently, the T_c values of salts **1** and **2** were compared to those of (HDABCO$^+$)(BF$_4$$^-$) and (HDABCO$^+$)(ClO$_4$$^-$) salts as reference. For the (HDABCO$^+$)(BF$_4$$^-$) and (HDABCO$^+$)(ClO$_4$$^-$) salts, the transition temperatures from the paraelectric to the ferroelectric state are 377 and 378 K, respectively, and the hydrogen-bonding N−N distances are 2.841 and 2.839 Å, respectively.[4] The average N−N distance of salt **1** ($d_{\text{N−N}} = 2.789$ Å) was shorter than those of (HDABCO$^+$)(BF$_4$$^-$ or ClO$_4$$^-$). Our results indicated that the difference in the average N−N distances (approximately 0.05 Å) is sufficient in decreasing the barrier height of the double-well potential curves of the proton coordinate, resulting in a significantly lower T_c value (306 K) than those of (HDABCO$^+$)(BF$_4$$^-$ or ClO$_4$$^-$). The deuterium isotope effects of the dielectric transitions for (HDABCO$^+$)(BF$_4$$^-$ or ClO$_4$$^-$) were not reported, and therefore, direct comparison of the deuterium isotope effect for the (HDABCO)$_\infty$ hydrogen-

bonding chain should be impossible. In the case of salt **2**, the average N−N distance ($d_{\text{N−N}} = 2.801$ Å) is comparable to that of salt **1** ($d_{\text{N−N}} \approx 2.79$ Å) rather than that of (HDABCO$^+$)(BF$_4$$^-$ or ClO$_4$$^-$) ($d_{\text{N−N}} \approx 2.84$ Å); however, the dielectric transition temperature of salt **2** was significantly higher than that of salt **1**. The large deuterium isotope effect of salts **1** and **2**, therefore, cannot be simply explained by the change in the hydrogen-bonding distances, which suggested the influences of the structural modulation of the 1D (DDABCO$^+$)$_\infty$ hydrogen-bonding chain or existences of TCNQ stacks. The result is comparable to the large deuterium isotope effect ($\Delta T \approx 90$ K) in hydrogen-bonding ferroelectric crystals of potassium dihydrogen phosphate (KDP).[3,15]

Conclusion

1D dielectric (N···H···N)$_\infty$ hydrogen-bonding chains of HDABCO$^+$ were introduced into the electrically conducting TCNQ salts as the countercation structure. For the (HDABCO$^+$)$_2$-(TCNQ)$_3$ salt, segregated nonuniform TCNQ stacks were observed as the electrically conducting column. At room temperature, (HDABCO$^+$)$_2$(TCNQ)$_3$ exhibited semiconductive behavior. Changes in the proton coordinates within the hydrogen bonds were strongly coupled to the dielectric phase transition within the TCNQ-based molecular semiconductor. Temperature-dependent X-ray structural analysis revealed thermally activated localization/delocalization (order/disorder) of the protons or deuteriums within the 1D hydrogen-bonding chains. The dielectric transition of (HDABCO$^+$)$_2$(TCNQ)$_3$ was observed at 306 K, at which temperature a large deuterium isotope effect was detected [$\Delta T_c = 70$ K for (DDABCO$^+$)$_2$(TCNQ)$_3$]. These conductive dielectric materials can be formed into novel electric molecular materials and can be potentially developed as dual memory devices.[16] When the dipole structures are arranged by applying an electric field, strong interactions between the dipole arrangements in the dielectric parts and the conductive electrons have a potential to induce nonlinear current−voltage characteristics. Preparations of new molecular dielectric materials possessing the open-shell electronic structures are currently in progress to fabricate novel molecular conductors.

Supporting Information Available: UV−vis−NIR spectra, electrical conductivities, solid state ^{13}C NMR, tables of crystal data, structure solution and refinement, atomic coordinates, bond lengths and angles, and anisotropic thermal parameters for salts **1** and **2** at 100 and 373 K (PDF, CIF). This material is available free of charge via the Internet at http://pubs.acs.org.

JA0377697

(15) Ichikawa, N.; Motida, K.; Yamada, N. *Phys. Rev. B* **1987**, *36*, 874.
(16) Hill, N. A. *J. Phys. Chem. B* **2000**, *104*, 6694.